MECHANICS AND MODELING OF FLOW, SEDIMENT TRANSPORT AND MORPHOLOGIC CHANGE IN RIVERINE LATERAL SEPARATION ZONES

Brandy Logan, Physical Scientist, USGS, Golden, CO, blogan@usgs.gov; Jonathan Nelson, Research Hydrologist, USGS, Golden, CO, jmn@usgs.gov; Richard McDonald, Hydrologist, USGS, Golden, CO; Scott Wright, Research Hydrologist, USGS, Sacramento, CA, sawright@usgs.gov.

Abstract Lateral separation zones or eddies in rivers are critically important features for sediment storage and for a variety of roles they play in riparian and aquatic ecology. As part of a larger effort to predict the morphology of lateral separation zones in the Colorado River in Grand Canyon for a selection of sediment supply and discharge scenarios, we evaluated the performance of two modeling techniques for predicting flow, sediment transport, and morphodynamics in eddies using field data. In order to understand the relative roles of various exchange mechanisms between the main channel and eddies, we applied two-dimensional unsteady and three-dimensional unsteady models in a reach containing a lateral separation zone. Both models were developed, calibrated, and evaluated using detailed field data comprising acoustic-Doppler velocity measurements, water-surface elevations, sediment concentration by size class, and bathymetry measured during a flood event in the Colorado River. Model results and measurements are used to develop a better understanding of the mechanics of water and sediment exchange between the eddy and the mainstem and other factors that control the morphology of the reach.

INTRODUCTION

Lateral separation zones or eddies below channel constrictions store sediment in the form of sand bars in the Grand Canyon (Figure 1). Backwaters that develop in eddy return channels (Schmidt, 1990) during lower flows may provide critical habitat for several endangered fish species and subaerially exposed portions of the sand bars provide surfaces for riparian vegetation that support associated fauna (Wright et al., 2005). The number and size of sand bars in Grand Canyon has declined since construction of Glen Canyon Dam in 1963 (Schmidt et al., 2004). The dam substantially altered the seasonal flow pattern of the Colorado River while capturing virtually all mainstem sediment, leaving the Paria and Little Colorado Rivers as the primary sources of sediment in the system (Topping et al., 2000; Topping et al., 2003; Wright et al., 2005).

Despite changes to dam operations in 1991 designed to reduce sand bar erosion, sand bars have continued to erode. High flow experiments (HFE) were conducted in 1996, 2000, 2004, and 2008 in an effort to rebuild depleted sand bars by transporting sediment stored on the bed to higher elevation portions of sand bars and channel margin deposits (Schmidt et al., 1999). The 2004 and 2008 HFE were timed to follow high sediment loads supplied to the Colorado River by the primary tributaries, so that more sediment was available in the river system for sand bar formation (Wright et al., 2005, U. S. Geological Survey 2007). There is considerable interest in determining whether or not high flow releases from Glen Canyon Dam have the capacity to restore sand bars that persist over longer time frames. This depends in part on determining the

optimum high flow hydrograph and sediment supply conditions for producing the largest increase in sand bar size and number in the canyon.

This study is part of a larger effort to use morphodynamic models to predict the morphology of lateral separation zones for a variety of sediment supply and discharge scenarios. Here we evaluate the performance of two different modeling techniques to assess the relative roles of different sediment-transport mechanisms between the main channel and eddies by using two-dimensional (2D) and three-dimensional (3D) unsteady models. The two models were compared using field data collected during the March 2008 HFE. The goals of the model comparison were to determine the level of physical complexity needed for modeling flow and morphologic change in eddies, and to further evaluate the incremental improvements offered by more complicated models as a function of the additional data and computational effort required. The performance of each model was evaluated by comparing their predictions of flow, sediment transport, and morphodynamics to measurements collected near river mile 44.5 (Figure 1).

Figure 1 Map of the study area on the Colorado River in Grand Canyon, showing primary tributaries.

2008 HIGH FLOW EVENT AND STUDY AREA

In March of 2008 an experimental high-flow was conducted in the Grand Canyon following substantial sediment inputs from tributaries. The HFE ramped up from an average flow of approximately 311 m^3/s over 36 hours to a peak discharge of approximately 1,211 m^3/s which lasted 60 hours, returning to a similar low flow over 28 hours (Figure 2).

Detailed measurements were made in the pool and eddy associated with the Eminence Break Camp near river mile 44.5 defined downstream from Lees Ferry, Arizona. Multibeam acoustic measurements of bed topography and Acoustic-Doppler Current Profiler (ADCP) surveys (Scott Wright, personal communication) of velocity were made before the high flow, twice per day during the high flow, and after the high flow event. Suspended-sediment samples were collected

by dip sample once per day in the pool near the downstream end of the study site during the high flow (Scott Wright, personal communication). Suspended-sediment concentration peaked early and subsequently fell to values less than half of the peak concentration during the HFE (Figure 2). Water-surface elevations determined from position data associated with the multibeam acoustic measurements were used in calibration of the models.

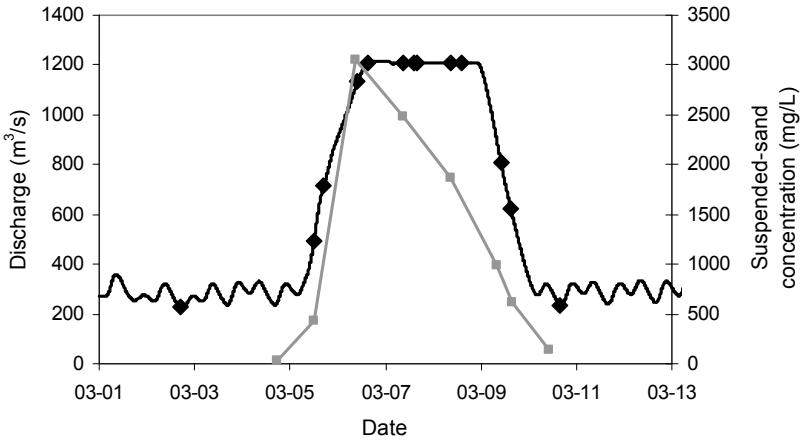

Figure 2 Discharge (black) and suspended-sediment concentration (grey) at the study site, March 2008. Black diamonds indicate the time of bathymetric surveys.

MORPHODYNAMIC MODELS

The Delft3D morphodynamic modeling system (version 3.28 Beta) was selected for this study because of its ability to model two- and three-dimensional flow for unsteady states. The model solves the nonlinear shallow-water equations for 2D and 3D turbulent flow (Lesser et al., 2004). In addition, this model includes options to calculate large-scale horizontal turbulent motions (Uittenbogaard and Van Vossen, 2004) which may be important for sand bar development. The model calculates bed load and suspended-load transport, suspended-sediment concentrations, and evolution of bed topography and bed sediment composition. Two different models were evaluated in this preliminary assessment, a vertically integrated 2D model and a 3D model. Both models used the Horizontal Large Eddy Simulation (HLES) which allows prediction of large scale unsteady horizontal eddies such as those found along the channelward margin of the eddy flow field (Uittenbogaard, 1998).

The modeled reach is approximately 800 m long and contains the rapid, pool and eddy associated with the Eminence sand bar (Figure 3). The same model reach and associated computational grid were used for both model scenarios. To reduce model computational time, a coarse grid of 70 x 24 gridlines was used; this is roughly equal to grid cells of 8 by 12 m with the long axis oriented downstream. The vertical dimension of the 3D model was specified using a sigma-grid which is bounded by the bed topography and the free water surface (Phillips, 1957). The sigma-grid contained 12 vertical layers of logarithmically decreasing thickness towards the bed.

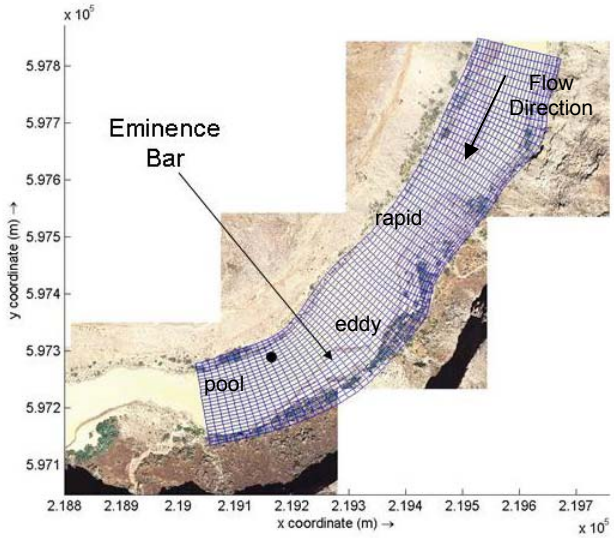

Figure 3 Air photo of the study reach showing the location of the Eminence sand bar. The computational grid used for all model runs is shown in blue. The black dot indicates where suspended-sediment samples were collected.

Model calibration Required model boundary conditions include the discharge at the upstream boundary and the elevation of the water surface at the downstream boundary. The discharge at the study site was estimated using a reach-averaged model of discharge wave propagation (Wiele and Smith, 1996). The water-surface profile for the lower half of the model reach is unusual in that it has an adverse grade, such that the water-surface elevation increases near the downstream boundary as the water decelerates and becomes super elevated on the outside of the bend. To account for this, we used a variable downstream water-surface elevation boundary based on water-surface measurements made during the calibration time period. The flow model also required an initial estimate of the water-surface which was set to a constant high value everywhere and allowed to relax as the solution converged.

The models were calibrated using the streambed topography measured near the end of the peak discharge without allowing the bed to evolve. In order to calibrate the models, we selected a range of roughness values representing simple grain-based roughness up to the amplitude of the average dune in the reach. The 3D model specifies roughness using z_0 values (parameter related to the physical roughness of the bed); corresponding *ks* roughness values (roughness proportional to grain size) calculated using $z_0=ks/30$ were used in the 2D model. These model results were then compared to water-surface elevations estimated using position and offset data from the multibeam acoustic measurements for the same day the calibration topography was surveyed. The modeled water-surface profiles were time-averaged over the duration of the peak discharge to obtain average conditions rather than water-surface elevations influenced by vortex shedding, which caused episodic changes in the water-surface profile. In addition, we evaluated the magnitude of the modeled depth-average velocity compared to measured data collected along cross-sections using an ADCP. Measured and modeled time-average velocity vectors were also compared to help determine which roughness values resulted in the best solution possible.

It was difficult to match the water-surface profile in the rapid above the eddy using a single value of roughness. Using variable roughness with higher values in the channel upstream from the bar improved model results to some extent, however even very high roughness values could not perfectly match the water-surface profile in the rapid. This is likely due to insufficiently defined topography in this region. However the upstream rapid could not be excluded from the model reach because the expansion of the channel below the rapid drives the distribution of flow and generates the eddy. We therefore used a two-part roughness that specified higher z_0 and *ks* values in the rapid portion of the reach upstream from the Eminence sand bar. This reduced the error in the water-surface through the rapid and improved the estimated water-surface in the eddy eye, which otherwise tended to be too high.

The best fit between measured and modeled water-surface and velocity data for the 3D model occurred using a z_0 of 0.001 in the main channel and 0.05 in the rapid upstream from the Eminence sand bar. The root mean square (RMS) error between the measured and modeled water surfaces under the calibration conditions was 0.028 m (Fig 4). The equivalent *ks* values of 0.03 and 1.5 appeared to work well in the 2D model given an RMS error of 0.043 m; however the 2D model was not very sensitive to different *ks* values. The RMS errors between the measured and modeled mean water velocities were 0.34 m/s and 0.36 m/s for the 3D and 2D models respectively (Figure 5).

Both models developed recirculating flow in the Eminence eddy and flow separation occurred at approximately the measured location, however the eddy eye was shifted upstream relative to measurements (Figure 6). In the eddy, the velocity vectors seem best represented by the 3D model as indicated by similar vector orientation and magnitude. The 2D modeled velocities were lower than the measured velocities indicating that the eddy was not as strongly defined by this model. However, in general both models produced reasonable hydrodynamic results, despite the fact that the 3D model is more complex and has substantially longer computational times.

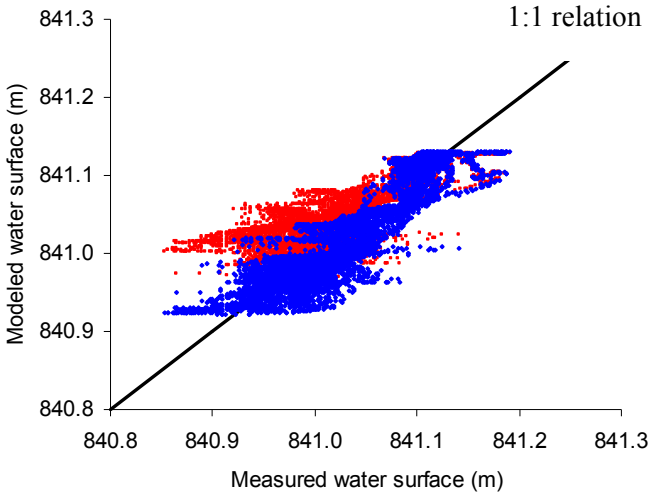

Figure 4 Measured and modeled water-surface elevations throughout the reach for the 2D (red) and 3D (blue) model.

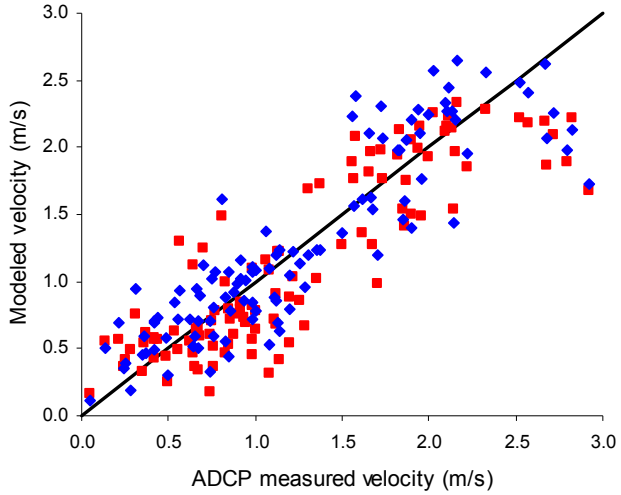

Figure 5 Measured and modeled mean water velocities throughout the reach for the 2D (red) and 3D (blue) model.

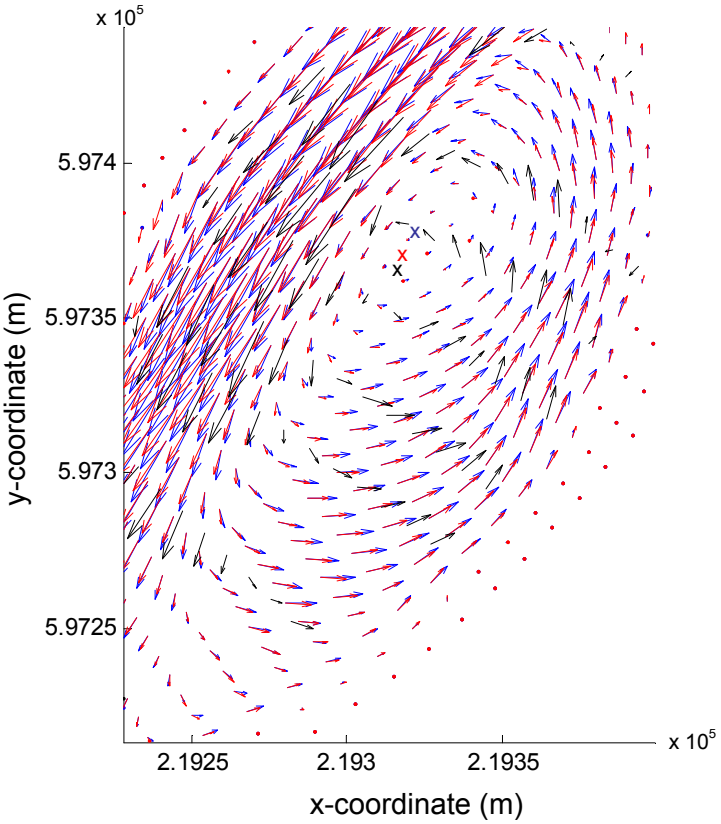

Figure 6 Measured and modeled water velocity vectors near the Eminence eddy. Black vectors show measured values, red show the 2D model, and blue show the 3D model results. The "x" shows the locations of measured and modeled eddy-eyes.

Morphodynamic model Once each model was calibrated, sediment-transport calculations were performed and the bed was allowed to evolve beginning with the topography measured prior to the HFE. The models were developed using a compressed hydrograph that simulated the shape

and magnitude of the actual hydrograph, but not the duration. The duration of the hydrograph was reduced by a factor of 6 which reduced the simulation time substantially (Deltares, 2009). Bed evolution was corrected to the actual duration of the peak by using a morphological time-scale factor.

An additional boundary condition for the sediment-transport calculations is the concentration of the suspended sediment entering the reach. The suspended-sediment concentration measurements made near the lower end of the reach were the only data available to specify the change in concentration through time at the upstream boundary. These data were classified into 5 size classes following Sloff et al. (2009) and compressed sediment concentration curves corresponding to the compressed hydrograph were developed for each class (Table 1).

Table 1 Classified grain sizes and fraction of the bed composition applied in the models.

	Grain size (mm)	Range (mm)	Fraction of the bed
Very fine sand	0.088	0.062-0.125	0.055
Find sand	0.176	0.125-0.250	0.405
Medium sand	0.354	0.250-0.500	0.458
Coarse sand	0.707	0.500-1.000	0.080
Very coarse sand	2.000	1.000-4.000	0.002

Initial conditions for the sediment-transport calculations include specification of the initial sediment concentration everywhere in the reach, the thickness of the material on the bed, and the initial bed grain size distribution. The initial suspended-sediment concentration for each grain size was set using the measured values at the start of the modeled time-frame. The sediment thickness provides both a potential source of sediment in the reach and a lower boundary for potential scour. The initial thickness at the beginning of the HFE was estimated by comparing the topography measured prior to the HFE to maps of the minimum elevation ever measured in the Eminence reach based on multiple surveys going back as far as the 1990s (Matt Kaplinski, personal communication). Locations lacking survey data did not get assigned a thickness value. This was reasonable given that most of these areas were located in the rapid which should not readily erode. The composition of the bed material has not been directly measured; however, the mean particle size of the bed surface was determined using photographic techniques (Rubin et. al., 2007). The initial size distribution was estimated by assuming log-normal distributions around the mean grain size based on a standard deviation, σ=1.6, estimated from composited sediment samples from the Eminence sand bar. This size distribution was then classified into the same 5 size classes used in the boundary conditions and the relative proportion of each size class was used to assign a proportional thickness of each sediment size on the bed spatially in the model (Table 1).

RESULTS

During the HFE, replicate measurements of topography showed deposition along the Eminence reattachment bar during the rising limb of the hydrograph (Scott Wright, personal communication). This was followed by a large failure along the entire edge of the bar that deposited a substantial amount of material in the main channel. This material was gradually

evacuated during the hydrograph peak and a dune field formed adjacent to the downstream end of the bar in the lower portion of the reach. Deposition occurred on the bar at higher elevations as the HFE progressed. In the eddy eye sediment alternately filled and scoured, which has been interpreted as mass failures when the deposit over-steepened.

Cumulative erosion and deposition maps developed over the coarse of the HFE hydrograph show that both models build two large bars into the main channel, one in the Eminence eddy and the other on river right near the downstream end of the modeled reach (Figure 7). Relative to the measured behavior, both the 2D and 3D morphodynamic models deposited too much sediment on the top of the reattachment bar, built the bar too far into the main channel, and deposited more sediment than was measured in the eddy eye. Both models also scoured a deep thalweg which extended through the modeled reach, whereas the measured topography showed deposition of a dune field near the downstream end of the modeled reach.

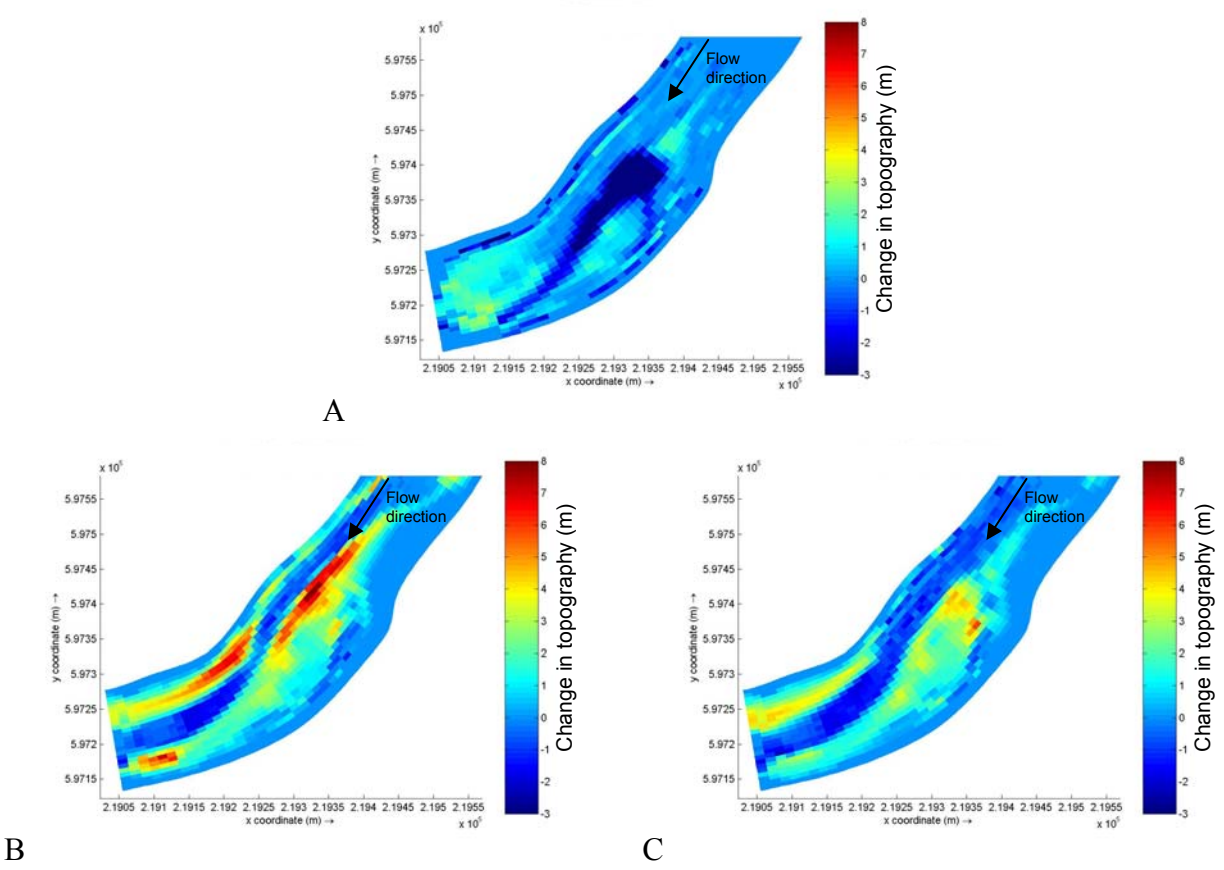

Figure 7 Cumulative erosion and deposition maps from just prior to the HFE to just after the HFE. A. shows the measured change, B the 2D modeled change and, C the 3D modeled change.

Analysis of cross-sections in the reach shows the extent to which the eddy eye and the bar are over-built by the 2D and 3D models (Figure 8). Panel B shows that at the end of the discharge peak, the sand deposited in the eddy eye had slumped reducing the measured elevation by more than 5 m in places, whereas the model results show the elevation of the bar increasing by several

meters. Panel C shows that both models deposited too much sediment on the bar and that the modeled return channel was not as deep as the measured return channel in both model runs.

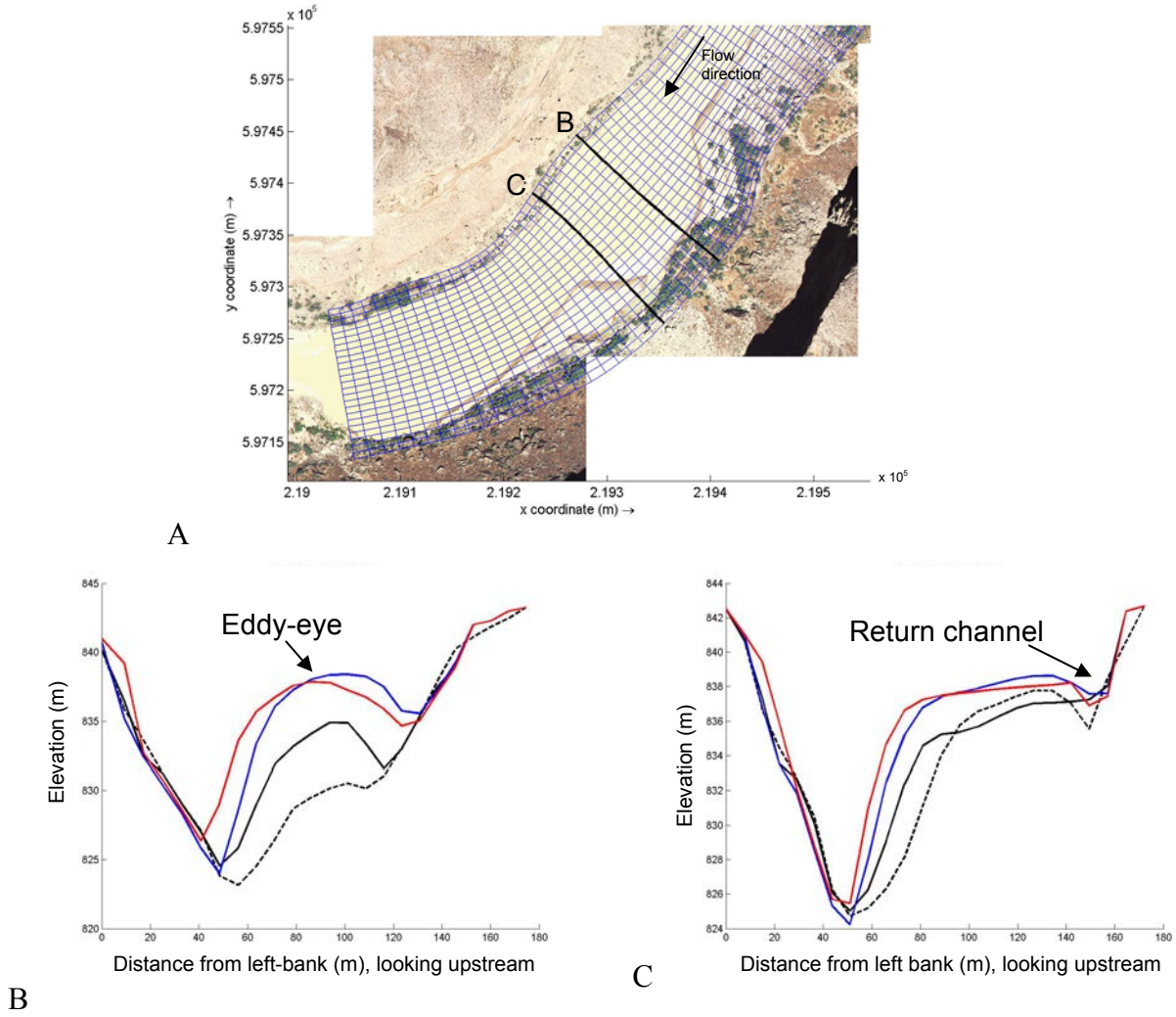

Figure 8 Panel A shows the relationship between the computational grid, the bar, and two cross-sections, B shows the upper cross-section which bisects the eddy-eye during the peak and C shows the lower cross-section on the bar. The solid black line denotes the initial topography, the dashed black line the post HFE topography, the red line shows the 2D, and the blue the 3D topography at the end of the HFE event.

DISCUSSION

Overall the 3D model better predicted the topography at the end of the HFE than the 2D model. The 2D model tended to build the reattachment bar and a bar on river left further into the main channel, build higher bars, and deposit more material in the thalweg at locations that typically remained about the same or scoured as indicated by measured topography. However, the 3D model displayed similar tendencies and failed to accurately predict the post-HFE topography.

Two factors appear to contribute to the over-development of the eddy bar, the first is related to slumping processes and the second to an over-supply of material to the eddy.

Subaqueous slump failures were measured during HFEs in 1996, 2000, and 2008 and appear to be an important process controlling the morphological response of this reach to high flows (Schmidt et al., 2004; Scott Wright, personal communication). These failures occurred on the rising limb of the hydrograph, suggesting that early deposition over-steepened the bar topography. The 2008 slump failure counteracted deposition in the eddy eye and margin of the bar to the extent seen in the model results. The modeled slope of the bed was much steeper on the edge of the bar than either the initial measured topography or the topography measured at the end of the HFE. The maximum measured bed slope on the bar was 25 degrees, whereas the maximum slope in the models was 35 degrees for the 3D model and 42 degrees for the 2D model. Because the angle of repose is between 26 and 34 degrees, the modeled topography was theoretically steep enough to fail, but this process is currently not incorporated in the morphodynamic model.

While slumping appears to be an important process that can not currently be accounted for by the models employed, the large spatial extent and high elevation of the modeled eddy bar suggested that the models computed excessive sediment supply to the eddy. We investigated a number of processes that could affect the sediment supply and final modeled topography by varying relevant model parameters. Occasionally model parameters were set to extreme values to determine the impact of that parameter on morphology.

Several processes did not appear to be important controls on the channel topography. Limited analysis indicated that topography was relatively insensitive to the size and composition of the bed material. The thickness or supply of material available on the bed also had negligible impact on the final topography. Artificially reducing the horizontal eddy diffusivity still resulted in too much deposition in the eddy, even when diffusivity was set to zero. This suggests that advection played a more important role than diffusion in transporting sediment into the eddy in the models.

Other processes did appear to exert substantial control on the modeled topography. Model conditions or parameters that controlled the concentration of sediment coming into the reach and the near-bed reference concentration greatly affected the results. In addition model conditions that affected advection in the model by altering the degree of local temporal variability in the flow, such as the horizontal eddy viscosity, also appeared to be important.

The near-bed reference concentration in the models is set by the van Rijn (1993) sediment transport model and simple estimates of this parameter using the method by Mclean (1992) suggested that the model calculated values were potentially high. However, further investigations of the reference concentration are necessary and may include examining other sediment-transport relations such as van Rijn (1984), or others.

Reducing the incoming sediment concentration substantially altered the modeled topography. Studies have shown that the Colorado River system is sensitive to sediment availability during HFEs (Topping et al., 2000 and Wright et al., 2005). Although the suspended-sediment concentration used in the model was not measured at the upstream end of the modeled reach, it is

unlikely that this value was substantially different given that similar values were measured upstream at river mile 30 and downstream at river mile 61(Grand Canyon Monitoring and Research Center sediment data available at http://www.gcmrc.gov/products/other _data, accessed on 2/9/2010).

Increasing the horizontal eddy viscosity above the values calculated by the HLES model effectively dampened strong temporal changes in the velocity and sediment flux vectors that intermittently deliver sediment into the eddy due to the unsteady nature of the 2D and 3D models. When horizontal eddy viscosity was low, sediment flux vectors were more frequently aligned toward the eddy, essentially forcing sediment into the eddy by advection. The models allowed this sediment to settle along the margin of the sand bar, rapidly forming a bar that extended too far into the main flow and had too high an elevation. This situation, compounded by the lack of slumping processes in the models, may provide a plausible explanation for the behavior of both the 2D and 3D morphodynamic models. Modeling the flow with steady 2D and 3D models, rather than adjusting the horizontal eddy viscosity to dampen temporal changes, may improve model results.

CONCLUSIONS

Preliminary modeling work indicates that properties of the flow field of lateral separation zones in Grand Canyon can be captured by both Delft 2D and 3D models (Lesser et al., 2004). The water-surface profile and velocity magnitude and vectors can be modeled relatively well using either method. However, both models have difficulty accurately predicting sediment transport and the resulting morphology of sandbars measured during the HFE in Grand Canyon. Both models over predict the amount of sediment deposited in the lateral separation zone and in other locations along the channel margin. Slumping of over-steepened sand bar deposits appears to be an important process that is not accounted for in the models. Model-calculated over-supply of sediment into the eddy through either advection or high sediment concentrations also appears to be a factor. More work on these factors, as well as other modeling options such as steady 2D and 3D models, is needed to determine whether or not more realistic results can be obtained.

REFERENCES

Delatres. (2009). “Simulation of multi-dimensional hydrodynamic flows and transport phenomena, including sediments: User manual”. Version 3.14, p. 384.

Lesser, G. R., Roelvink, J. A., van Kester, T, M., and Stelling, G. (2004). “Development and validation of a three-dimensional morphological model”, Journal of Coastal Engineering, 51, pp 883-915.

McLean, S.R. (1992). “On the calculation of suspended load for noncohesive sediments”, Journal of Geophysical Research, 97(C4), pp 5759-5770.

Phillips, N. A. (1957). “A coordinate system having some special advantages for numerical forecasting”, Journal of Meteorology, 14, pp 184-185.

Rubin, D. M., Chezar, H., Harney, J.N., Topping, D.J., Melis, T.S., and Sherwood, C.R. (2007). “Underwater microscope for measuring spatial and temporal changes in bed-sediment grain size”. Sedimentary Geology, 2002, pp 402-408.

Sloff, K, Wright, S, and Kaplinski, M. (2009). "High resolution three dimensional modeling of river eddy sandbars, Grand Canyon, U.S.A.", *in* Proceedings of the 6th symposium on River Coastal and Estuarine Morphodynamics, Santa Fe, Argentina.

Schmidt, J.D. (1990). "Recirculating flow and sedimentation in the Colorado River in Grand Canyon, Arizona", Journal of Geology, 98, pp 709–724.

Schmidt, J.C., Andrews, E.D., Wegner, D.L., Patten, D.T., Marzolf, G.R., and Moody, T.O., (1999). "Origins of the 1996 controlled flood in Grand Canyon", *in* Webb, R.H., Schmidt, J.C., Marzolf, G.R., and Valdez, R.A., eds., The controlled flood in Grand Canyon: Washington, D.C., American Geophysical Union, Geo-physical Monograph Series, 110, pp 23–36.

Schmidt, J.C., Topping, D.J., Grams, P.E., and Hazel, J.E., Jr. (2004). "System-wide changes in the distribution of fine sediment in the Colorado River corridor between Glen Canyon Dam and Bright Angel Creek, Arizona": Grand Canyon Monitoring and Research Center final report [http://www.gcmrc. gov/library/reports/physical/Fine_Sed/ Schmidt2004.pdf].

Topping, D.J., Rubin, D.M., and Vierra, L.E., Jr. (2000). "Colorado River sediment transport: pt. 1: natural sediment supply limitation and the influence of Glen Canyon Dam", Water Resources Research, 36, pp. 515–542.

Topping, D.J., Schmidt, J.C., and Vierra, L.E., Jr. (2003). "Computation and analysis of the instantaneous-discharge record for the Colorado River at Lees Ferry, Arizona, May 8, 1921, through September 30, 2000", U.S. Geological Survey Professional Paper 1677, [http://pubs.water.usgs.gov/pp1677].

Uittenbogaard R. E. and van Vossen, B. (2004). "Subgrid-scale model for quasi-2D turbulence in shallow water", in Jirka and Uijttewaal (Eds) Shallow Flows, Taylor and Francis.

Uittenbogaard, R. E. (1998). "Model for eddy diffusivity and viscosity related to sub-grid velocity and bed topography", Technical report.

U.S. Geological Survey, (2007). "Science plan for potential 2008 experimental high flow at Glen Canyon Dam", Flagstaff, Ariz., Southwest Biological Science Center, Grand Canyon Monitoring and Research Center.

Van Rijn, L. C. (1984). "Sediment transport, part I: bed load transport", Journal of Hydraulic Engineering, 110(10), pp 1431–1456.

Van Rijn, L. C. (1993). Principles of fluid flow and surface waves in rivers, estuaries, seas and oceans. Aqua Publications, The Netherlands.

Wiele, S. M., and Smith, J. D. (1996). "A reach-averaged model of diurnal discharge wave propagation down the Colorado River through the Grand Canyon", Water Resources Research, 32(5), pp 1375-1386.

Wright, S. A., Melis, T. S., Topping, D. J., Rubin, D. M. (2005). "Influence of Glen Canyon Dam operations on downstream sand resources of the Colorado River", in Gloss, S.P., Lovich, J.E., and Melis, T.S., eds., The state of the Colorado River ecosystem in Grand Canyon, U.S. Geological Survey Circular 1282, pp 17-31.